Extended-range order in tetrahedral amorphous semiconductors: The case of amorphous silicon

Devilal Dahal,[1,*] Stephen R. Elliott,[2,3,†] and Parthapratim Biswas[1,‡]

[1]*Department of Physics and Astronomy, The University of Southern Mississippi, Hattiesburg, Mississippi 39406, USA*
[2]*Physical and Theoretical Chemistry Laboratory, University of Oxford, Oxford OX1 3QZ, United Kingdom*
[3]*Department of Chemistry, University of Cambridge, Cambridge CB2 1EW, United Kingdom*

(Received 27 September 2021; revised 23 January 2022; accepted 24 February 2022; published 10 March 2022)

This paper reports the presence of extended-range ordering in the atomic pair-correlation function of amorphous silicon (*a*-Si) using ultralarge atomistic models obtained from Monte Carlo and molecular-dynamics simulations. The extended-range order manifests itself in the form of radial oscillations on the length scale of 20–40 Å, which is examined by directly analyzing the radial distribution of atoms in distant coordination shells and comparing the same with those from a class of partially ordered networks of Si atoms and disordered configurations of crystalline silicon from an information-theoretic point of view. The effect of the oscillations on the first sharp diffraction peak (FSDP) in the structure factor is addressed by obtaining a semianalytical expression for the static structure factor of *a*-Si, and calculating an estimate of the error of the intensity of the FSDP associated with the truncation of radial information from distant shells. The results indicate that the extended-range oscillations do not have any noticeable effects on the position and intensity of the FSDP, which is primarily determined by the medium-range atomic correlations of up to a length of 20 Å in amorphous silicon.

DOI: 10.1103/PhysRevB.105.115203

I. INTRODUCTION

The structure of amorphous silicon (*a*-Si) is well represented by the continuous random network (CRN) model of Zachariasen [1]. The CRN model of *a*-Si suggests that each atom is bonded to four neighboring Si atoms, which form an approximate tetrahedral atomic arrangement in the amorphous environment. The network is topologically distinct from its crystalline counterpart (*c*-Si) owing to the presence of five-member and seven-member rings. In addition, a considerable number of hexagonal rings and a few higher-member rings are also present in the amorphous network. The pair-correlation function (PCF) of *a*-Si obtained from CRN models indicates that radial correlations typically extend up to a distance of 15 Å. Although the actual structure of laboratory-grown samples of *a*-Si may differ from this simple CRN picture, except for a few properties, the CRN model provides an overall good description of structural, electronic, and vibrational properties of *a*-Si that mostly rely on the short-range order (≈5 Å) and, to a lesser extent, the medium-range order (≈5–20 Å) of the network.

Although the structure of *a*-Si has been extensively studied by using computer-generated models on the radial length scale of 10–15 Å, there exist only a few studies [2–5] that discuss the network structure of *a*-Si on the medium-range length scale of 20 Å and beyond. This is partly due to the fact that structural and electronic properties of *a*-Si are generally found to be not particularly dependent on the medium-range structure beyond 15 Å and in part to the computational complexity of conducting quantum-mechanical calculations, using density-functional theory (DFT), for large models. However, this observation does not necessarily imply that no medium-range structure exists in *a*-Si [6]. In this paper, we address this aspect of the problem by studying the network structure of *a*-Si using atomistic models of sizes 21 952 and 400 000 atoms. In particular, we examine two important aspects of the medium- and extended-range structures of *a*-Si that have been reported in the literature. The first problem involves the presence of weak but noticeable radial oscillations in the PCF at distances of 20–40 Å. This was first reported by Uhlherr and Elliott [7] and it was given the name extended-range oscillations in the PCF of *a*-Si. The second issue is directly related to the first and it concerns the effect of the medium-range order beyond 15 Å, and possibly the extended-range order, on the first sharp diffraction peak (FSDP) of *a*-Si. The latter corresponds to the first peak of the static structure factor [8], $S(Q)$, at $Q = 1.99$ Å^{-1} in *a*-Si. In the following, we use the term medium-range order (MRO) to imply ordering on the length scale of 5–20 Å, whereas the term extended-range order (ERO) indicates structural ordering beyond 20 Å, including extended-range oscillations.

The role of MRO in amorphous networks has been studied extensively in an effort to understand structure-property relationships in network-forming glasses, for example, oxides [9–13] and chalcogenides [14–18]. The MRO in these systems typically manifests itself as the FSDP, and the position, width, and intensity of the FSDP characterize the length scale associated with the MRO. The results from numerous experimental [11,19–24] and computational studies [2,25–30] indicate that the MRO and ERO in glassy systems can extend up to a distance of 30 Å and that it can play an important role

*devilal.dahal@usm.edu
†stephen.elliott@chem.ox.ac.uk
‡Corresponding author: partha.biswas@usm.edu

in determining a number of material properties of network-forming glasses. By contrast, results for tetrahedrally bonded elemental amorphous semiconductors, such as *a*-Si and *a*-Ge, are few and far between. Uhlherr and Elliott [7] studied the presence of extended-range oscillations in *a*-Si by analyzing experimental neutron-diffraction data of Fortner and Lannin [31] and the pair-correlation data obtained from atomistic models of size 13 824 atoms. [32] The authors concluded, via the Fourier inversion of the structure factor in the vicinity of the FSDP region, that the radial oscillations can extend to at least 35 Å and that it arises from the propagation of second-neighbor radial atomic correlations. Recently, Roorda *et al.* [33] reported the presence of ERO in amorphous Si/Ge using x-ray diffraction measurements at high resolution. The PCF obtained in their study from the Fourier transform of diffraction data shows the presence of ERO beyond 20 Å in both *a*-Si and *a*-Ge samples. The authors also noted that the (spatial) periodicity and decay length of the MRO and/or ERO increase upon thermal annealing. In view of these observations, the main task of the present study is to examine the presence of the ERO in large realistic models of *a*-Si by a direct analysis of the pair-correlation function and their partial counterparts associated with distant coordination shells of amorphous silicon.

The rest of the paper is arranged as follows. In Sec. II, we have provided a description of the computational methods employed here to generate atomistic models of *a*-Si and a set of partially ordered networks of Si atoms. This is followed by results and discussion in Sec. III. The origin of the ERO is addressed from a real-space point of view of the network structure of amorphous silicon. The relation between the ERO and structure of the FSDP is also examined in this section by constructing a semiempirical expression for the structure factor of *a*-Si in the Gaussian approximation. This is followed by conclusions of our work in Sec. IV.

II. COMPUTATIONAL METHOD

The present study involves the use of three different sets of models. The first set consists of *a*-Si models obtained from using the Wooten-Winer-Weaire (WWW) [34,35] algorithm. The second set comprises *a*-Si models produced from large-scale molecular-dynamics (MD) simulations. The third set includes three different types of partially ordered networks of Si atoms, denoted by M1, M2, and M3. These networks are not realistic models of *a*-Si; they have varying degrees of radial ordering in the respective PCF up to a radial length of 6 Å. In order for the ERO to manifest in the PCF of *a*-Si at radial distances of 20–40 Å, it is necessary for the models to be sufficiently large, consisting of a few tens to several tens of thousands of atoms. To this end, the sizes of the models were chosen to be 21 952 atoms and 400 000 atoms, which suffice to establish an unambiguous presence of the ERO in the PCF. In this study, we generated a set of three independent M1/M2/M3 and WWW models and three MD models for the purpose of configurational averaging of data.

The MD models were produced by initially placing 400 000 Si atoms randomly in a cubic simulation cell of length 202.4 Å, so that no two atoms could be at a distance of less than 2 Å. The mass density of the models corresponds to 2.26 g cm^{-3}, which is close to the experimental value [36,37] of the *a*-Si density, 2.25–2.28 g cm^{-3}, depending upon the method of preparation and experimental conditions. The modified Stillinger-Weber potential [38,39] was used to calculate the total energy and forces and the velocity-Verlet algorithm was employed to integrate the equations of motion in canonical ensembles. The initial temperature was set at 1800 K and the system was equilibrated for 20 ps at 1800 K. The temperature was then gradually decreased, by using a chain of Nosé-Hoover thermostats [40,41], from 1800 to 300 K at an average cooling rate of 5×10^{12} K/s. The final structures from the MD simulations were further subjected to geometry optimization using the limited-memory Broyden-Fletcher-Goldfrab-Shanno (BFGS) algorithm, as described by Atta-Fynn and Biswas [42]. Atomic configurations were collected during the course of simulations once the configurations satisfied a set of convergence properties, involving a minimum value of the width of the bond-angle distribution and the number of four-fold-coordinated atoms in the network.

The second set of models was produced by using the WWW method. Here, we employed the modified version of the algorithm, developed by Barkema and Mousseau [35]. The method essentially consists of the following steps:

(1) Generate a random configuration and construct a neighbor list of atoms using an appropriate cutoff value, such that the network is tetravalent as far as the list is concerned.

(2) Employ the WWW bond-switching algorithm [34,35] to produce a new configuration and accept or reject the configuration upon local relaxation of the network via the Monte Carlo method. The bond-switching procedure largely maintains the tetravalent character of the atomic network during simulations, and local relaxations were performed by using the nearest-neighbor-based Keating potential [43].

(3) Relax the resulting configuration from step 2 at a regular but infrequent interval to include the structural information from beyond the first shell of neighbors, by using a generalization of Weber's adiabatic bond-charge model [44].

For a description of the method, see Ref. [35]. In this study, we have employed three independent 21 952-atom WWW models for obtaining configurationally averaged values of structural properties. The atomic coordinates of the WWW models are provided as Supplemental Material [45].

In addition to the WWW and MD models of *a*-Si, we have also generated a set of disordered networks, M1–M3, of Si atoms. As stated earlier, these models are partially ordered and they can be classified by the degree of radial correlations present in the respective PCF. Specifically, M1 models are highly disordered and have very little or no radial correlations in the PCF. By contrast, M2 models are characterized by the presence of a well-defined first peak and radial correlations up to 3 Å. Likewise, M3 models exhibit radial correlations up to 6 Å with a pristine first peak and a part of the second peak, with a well-defined gap between the peaks. The M2 and M3 models were generated by adding one atom at a time in the simulation cell so that the addition of each atom satisfied a set of geometric constraints in order to produce radial correlations up to a length of 4 Å and 6 Å, respectively. The sizes of the

WWW and M1/M2/M3 models were chosen to be 21 952 atoms, with a cubic supercell of linear size 77.03 Å.

Apart from the WWW, MD, and M1–M3 models, we have also employed a number of disordered amorphous silicon (*da*-Si) and disordered crystalline silicon (*dc*-Si) configurations in this study. These configurations were produced by including structural disorder in pristine *a*-Si and diamond *c*-Si structures via random displacements of atoms, using $r_{i,\alpha} \rightarrow r_{i,\alpha} + \sigma\, p_{i,\alpha}$, from their original positions. Here, $r_{i,\alpha}$ is the αth component ($\alpha = x/y/z$) of the atomic position at site i, σ is the maximum value of the atomic displacement in angstroms, and $p_{i,\alpha}$ is a random number, which is uniformly distributed between -1 and $+1$. The values of σ were chosen from 0.2 to 1.2 Å, which correspond to a distortion of the Si–Si bond length by 8–51% from its average or ideal value of 2.36 Å in *a*-Si or *c*-Si. It may be noted that a value of σ of the order of 0.3 Å satisfies the Lindemann criterion of melting, producing liquidlike structures of *a*-Si and *c*-Si. Thus, the *dc*-Si configurations with $\sigma \gg 0.3$ Å are considerably disordered compared to their counterparts with $\sigma \leqslant 0.3$ Å.

Given a distribution of atoms in a disordered network, the structure factor can be obtained from the Fourier transform of the reduced PCF, $G(r)$. Assuming that the distribution of atoms in the network is homogeneous and isotropic, the structure factor, $S(Q)$, is given by

$$S(Q) = 1 + \frac{4\pi n_0}{Q}\int_0^{\infty} r[g(r)-1]\sin(Qr)\,dr \approx 1 + \frac{1}{Q}\int_0^{R_c} G(r)\sin(Qr)\,dr, \quad (1)$$

where $g(r)$ is the conventional PCF, $G(r) = 4\pi n_0\, r\,[g(r)-1]$ is known as the reduced PCF, and n_0 is the average number density of the system. For finite-size models, the upper limit of the integral can be replaced by $R_c = L/2$ by using the periodic boundary conditions, provided $g(r) \rightarrow 1$ as $r \rightarrow R_c$. We see later that this condition is amply satisfied by models for which R_c is of the order of 20 Å.

III. RESULTS AND DISCUSSION

A. Extended-range oscillations in the PCF of *a*-Si

We begin by establishing the unambiguous presence of radial oscillations in the PCF of *a*-Si at a distance of 20–40 Å. Since the calculation of the PCF beyond 20 Å requires sufficiently large models of *a*-Si, we first examine the large MD models, consisting of 400 000 atoms. Thereafter, we proceed to determine the origin of these oscillations by analyzing the three-dimensional network structure of these 400 000-atom models and a set of 21 952-atom models obtained from the WWW method. The results from these models will be compared with the same from the partially ordered networks, M1–M3, having varying degrees of radial ordering up to a distance of 6 Å. The PCFs of the partially ordered networks, from M1 to M3, are shown in Fig. 1, along with the results from the 21 952-atom WWW models of *a*-Si. It is evident from the plots that the M2 and M3 models show radial correlations of up to 4 and 6 Å, respectively. The M1 models, on the other hand, exhibit small radial correlations up to 3 Å, which mostly originate from the imposed constraint of a minimum separation distance of 2 Å between any two atoms in the network.

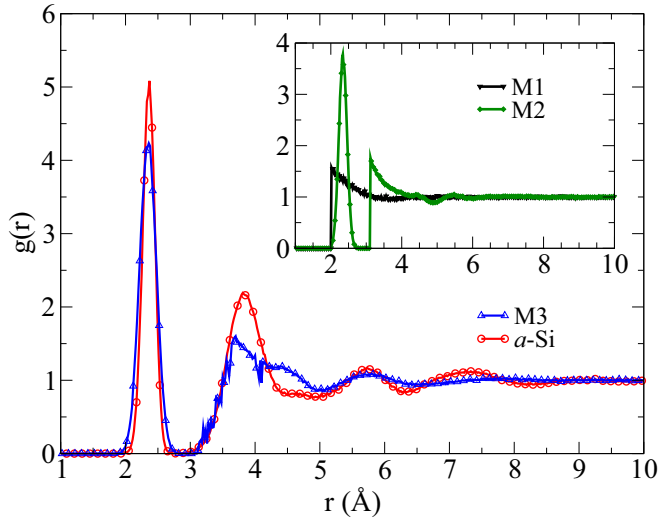

FIG. 1. The pair-correlation functions of three partially ordered models (M1–M3) of Si atoms, showing radial correlations up to a length of 6 Å. The results for *a*-Si (WWW models) are shown for comparison with that for the M3 model. The size of the models corresponds to 21 952 atoms and the PCF data were averaged over three independent configurations for each model.

Figure 2 shows the reduced PCF obtained from the MD models of *a*-Si, which consist of 400 000 atoms. The data presented here correspond to the configurational-averaged values of $G(r)$ from three independent configurations. The inset in Fig. 2 shows the presence of distinct radial oscillations at a distance beyond 20 Å, extending at least up to 40 Å. Similar oscillations have been also observed in the reduced PCF of 21 952-atom WWW models, but in a somewhat weaker form.

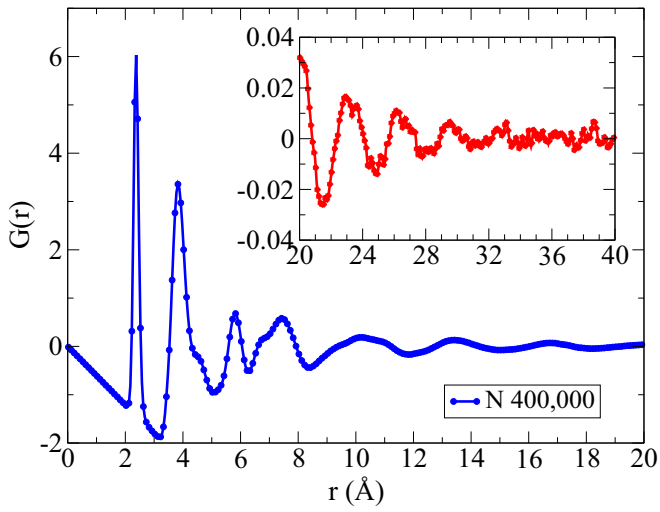

FIG. 2. The reduced pair-correlation function, $G(r)$, of *a*-Si, obtained from a configurational averaging of three large MD models of size 400 000 atoms. The inset shows the presence of radial oscillations up to 40 Å, which are known as the extended-range oscillations in *a*-Si.

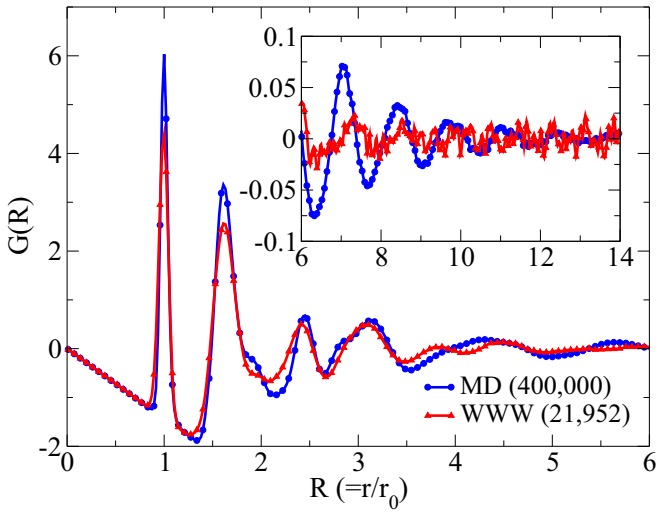

FIG. 3. The reduced PCFs of the 400 000-atom MD models and 21 952-atom WWW models showing the presence of considerable extended-range oscillations in larger MD models. For clarity, the radial distances are scaled by the corresponding first peak of the PCF, i.e., $R = r/r_0$, where $r_0 = 2.37$ Å.

This is apparent in Fig. 3, where we have plotted the configurationally averaged reduced PCFs for the 400 000-atom MD models and 21 952-atom WWW models. For comparison, the radial distances (r) in Fig. 3 are scaled by the corresponding position of the first peak (r_0) by introducing a scaled variable $R = r/r_0$. The inset in Fig. 3 clearly shows the presence of considerable oscillations in larger 400 000-atom MD models compared to their WWW counterpart in the region of R from 6 to 14, which translates into a distance of 14 to 33 Å for $r_0 \approx 2.37$ Å. The observed differences can be partly attributed to the size and statistics and in part to the nature of simulations. In general, MD models are considered to be more representative of annealed samples of a-Si, which are slightly more ordered than their as-deposited counterpart.

Table I presents some characteristic structural properties of the MD and WWW models. Since the presence of too many structural defects can affect the local density of the networks, and the radial correlations between atoms, it is necessary for the models to exhibit properties that are compliant with experimental observations. The presence of only a few dangling bonds (up to 1.3%) and floating bonds (up to 1.2%), as well as a small value of the root-mean-square width, $\Delta\theta$, about 9–10°, of the bond-angle distribution, confirms that the structural properties of these models are indeed consistent with actual samples of a-Si.

TABLE I. Structural properties of three WWW models (W1–W3) and three MD models (MD1–MD3). The average bond length ($\langle r\rangle$), average bond angle ($\langle\theta\rangle$), and the root-mean-square width of bond angles ($\Delta\theta$) are expressed in Å and degrees, respectively. C_n indicates the number of n-fold-coordinated atoms (in percent).

Model		Bond angle		Atomic coordination				Bond length
Type	Size (N)	$\langle\theta\rangle$	$\Delta\theta$	C_2	C_3	C_4	C_5	$\langle r\rangle$
W1	21 952	109.21	10.04	0.00	0.00	99.86	0.14	2.36
W2	21 952	109.23	9.83	0.00	0.00	99.9	0.1	2.36
W3	21 952	109.22	9.87	0.00	0.00	99.88	0.12	2.36
MD1	400 000	109.23	9.26	0.02	1.28	97.59	1.11	2.38
MD2	400 000	109.23	9.31	0.03	1.29	97.52	1.16	2.38
MD3	400 000	109.23	9.34	0.02	1.26	97.57	1.15	2.38

To further characterize the models, one often computes the electronic density of states (EDOS). The EDOS in a-Si is found to be very sensitive to the presence of coordination defects, especially three-fold-coordinated Si atoms or dangling bonds. The presence of an electronic gap largely depends on these defects, and the size of the gap is known to be related to the density of such defects and the degree of disorder in bond-length and bond-angle distributions. We have therefore calculated the EDOS of 21 952-atom WWW models and 400 000-atom MD models. Since the diagonalization of the Hamiltonian matrix (H) of such large a-Si models is highly nontrivial, we had to resort to (a) the tight-binding approximation of the Hamiltonian; and (b) employing the recursion method of Haydock, Heine, and Kelly (HHK) [46,47] to obtain the EDOS. In the recursion approach of HHK, one calculates the projected density of states $n_\alpha(E)$, associated with a basis function $|\alpha\rangle$ (involving a site and an orbital), by writing

$$n_\alpha(E) = \sum_k |\langle\alpha|\psi_k\rangle|^2 \delta(E - E_k). \tag{2}$$

Here, E_k and ψ_k are the energy eigenvalues and eigenvectors of H, respectively. Using a representation of the δ function and writing $z = E + \imath\epsilon$, where $\epsilon \to 0^+$, it can be shown that the projected EDOS can be expressed in terms of the singular part of the diagonal element of the resolvent of H or the Green's operator $\hat{G}(z) = (z\hat{I} - \hat{H})^{-1}$. This yields [48]

$$n_\alpha(E) = -\frac{1}{\pi} \lim_{\epsilon\to 0^+} \mathrm{Im}\, G_{\alpha\alpha}(E + \imath\epsilon). \tag{3}$$

The local EDOS obtained from using Eq. (3) is averaged over multiple sites to calculate the total EDOS. For 400 000-atom MD models, the problem is particularly difficult due to the handling and storage of large matrices and the computational cost associated with the calculation for all sites. In practice, a few clusters of several hundred atoms are found to suffice for configurational averaging. Using a fast matrix-vector multiplication scheme and a compressed representation of the sparse H matrix, one can implement an order-N algorithm for the calculation of the local EDOS in the tight-binding approximation. The results obtained from these calculations are shown in Fig. 4. The presence of a clean gap, rather than a pseudogap, in the EDOS further establishes the quality of the models. The approach can be adapted to calculate the vibrational density of states in the harmonic approximation, provided that an efficient scheme to obtain electronic forces for the construction of the dynamical matrix (DM) of a-Si is available. A simple order-N approach to construct the DM can be found in Ref. [49].

B. Origin of extended-range oscillations in a-Si

The first step toward understanding the ERO in a-Si follows from an analysis of the reduced PCF of disordered

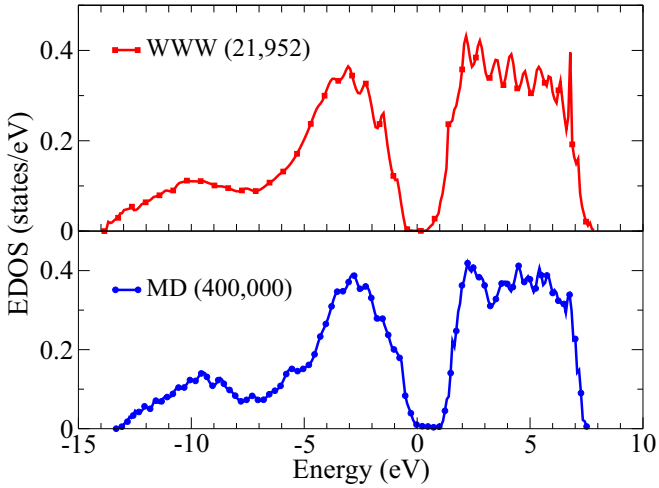

FIG. 4. The electronic density of states (EDOS) of 21 952-atom WWW and 400 000-atom MD models obtained from the tight-binding approximation. The presence of an electronic band gap is clearly visible in the plots.

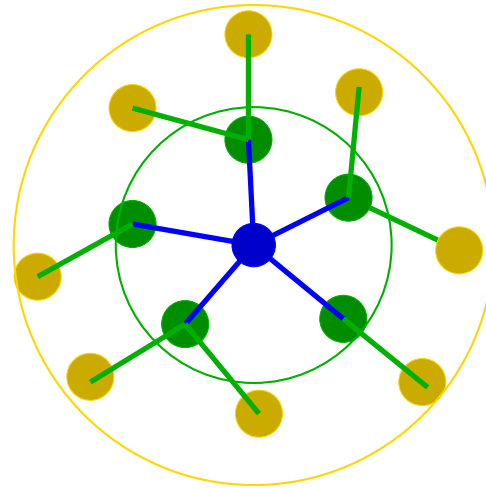

FIG. 6. A schematic representation showing the first two coordination shells of a central atom (blue) in a two-dimensional disordered network. The atoms in the first shell (green) and the second shell (yellow) can be reached from the central atom in one step and two steps, respectively.

crystalline silicon (*dc*-Si) structures. The inclusion of positional disorder washes out the sharp δ functions in the PCF of diamond *c*-Si and leads to a series of broadened peaks for the resulting *dc*-Si structures. A comparison of the reduced PCF of *a*-Si with those from *dc*-Si, for $\sigma = 1.0$ and 1.2 Å, in Fig. 5 reveals that *a*-Si exhibits small but noticeable oscillations at large distances of up to at least 30 Å. Despite the fine structure of $G(r)$ in *dc*-Si, it is apparent that the positions of the peaks in *a*-Si approximately coincide with those in *dc*-Si. This observation leads to the possibility that the ERO in *a*-Si could originate from the presence of weak radial-shell structures on the nanometer length scale, as in the case of *dc*-Si. This point is examined at length in the following paragraphs.

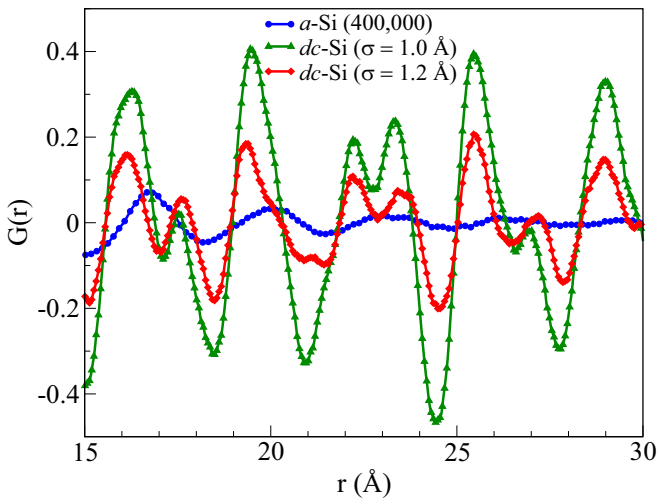

FIG. 5. The presence of radial oscillations in MD models of *a*-Si (blue) of size 400 000 atoms and two *dc*-Si structures of size 405 224 atoms from 15 to 30 Å. The positions of the radial peaks of *a*-Si approximately correspond to those of *dc*-Si, indicating the possible presence of weak extended-range ordering in *a*-Si beyond 15 Å.

Assuming that radial-shell structures exist in the partially ordered environment of *a*-Si at large distances, one may express the total PCF, $g(r)$, as a linear combination of the same for each coordination shell, $g_n(r)$. Thus, $g(r) = \sum_n g_n(r)$, where $g_n(r) = \langle g(r = |\mathbf{r_n} - \mathbf{R_i}|)\rangle_i$. Here, r is the distance between a central atom at $\mathbf{R}_i$ and its neighbors in the nth coordination shell at $\mathbf{r}_n$, and the symbol $\langle\,\rangle_i$ stands for the average over all atoms and independent configurations. Since, for an arbitrary (highly) disordered network, distant radial shells may not exist or be well defined—depending on the degree of radial disorder—it is more appropriate to define the nth coordination or topological shell as one that consists of nth-nearest neighbors of the central atom at $\mathbf{R_i}$. This is schematically illustrated in Fig. 6 by showing the first-shell neighbors (green) and the second-shell neighbors (yellow) of the central atom (blue). The key point here is that the nth neighbors of a central atom are those that can be reached (from the center) by a minimum of n distinct and irreversible steps, irrespective of the presence of well-defined radial shells. Thus, the coordination shells defined above depend on the topology or connectivity of the atomic network, and the three-dimensional shape of the shells may not be necessarily spherical. We see later that this can lead to a highly asymmetrical radial distribution of atoms within the coordination shells of partially disordered networks. Figure 7 shows the shell PCFs, $g_n(r)$, obtained for the first six coordination shells, along with $g(r)$ for a 21 952-atom WWW model of *a*-Si. It is apparent that the shell PCFs, for $n = 1$ to $n = 6$, can be represented by a bell-shaped curve in *a*-Si, with the exception of $g_3(r)$ for which a bimodal distribution is observed. The latter is consistent with the earlier study by Uhlherr and Elliott [7], who attributed the bimodal shape of $g_3(r)$ to the end-to-end radial distances of a set of four neighboring atoms or quartets associated with dihedral angles in *a*-Si.

Having expressed the total PCF in terms of $g_n(r)$, we now examine the oscillations in the PCF by studying individual

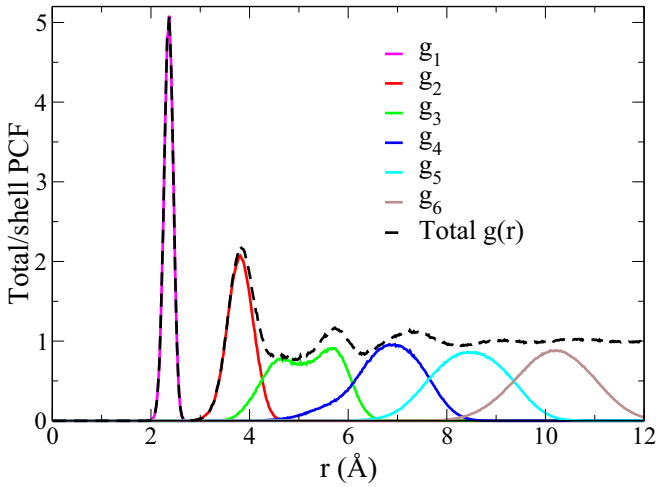

FIG. 7. The shell pair-correlation function, $g_n(r)$, for the nth coordination shell of a 21 952-atom WWW model of a-Si. The total $g(r)$ (dashed black), which is given by the sum of all shell PCFs, is also shown in the plot.

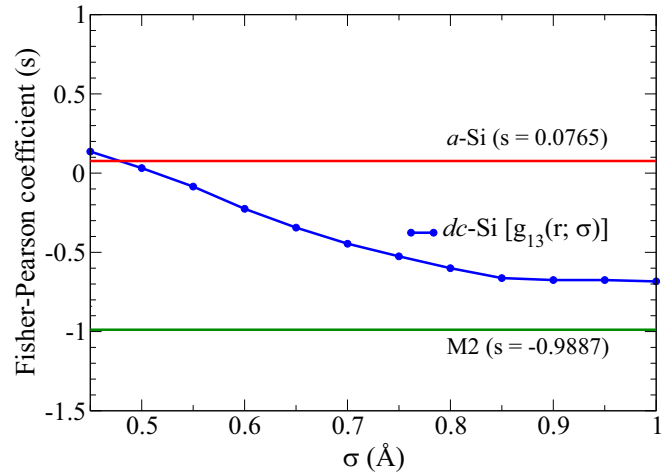

FIG. 9. The variation of the Fisher-Pearson coefficient of skewness, s, for the distribution $g_{13}(r;\sigma)$ with σ for a number of dc-Si models (blue). The coefficients for the M2 model (green) and a-Si (red), for $\sigma = 0$, are shown in the plot for comparison.

$g_n(r)$s, which reflect the characteristic properties of the radial distributions of atoms in nth shells. In particular, the width of $g_n(r)$ is indicative of the strength of the radial (dis)order in the nth shell. A small value of the width corresponds to a highly ordered state of atoms within the shell as far as radial ordering is concerned, and vice versa. This assertion can be verified by computing $g_n(r)$ for a number of partially ordered networks of silicon. Figure 8 shows the results for the 13th coordination shell, $g_{13}(r)$ as a representative example, obtained from 21 952-atom models, of a-Si, dc-Si, and M2. As stated earlier in Sec. II, the latter model (M2) is characterized by the presence of a well-defined first-coordination shell, whereas the dc-Si structures are produced by using a value of σ in the range from 0.3 to 1.0 Å. It is apparent that a small value of σ (for example, $\sigma = 0.3$ Å) produces well-defined multiple

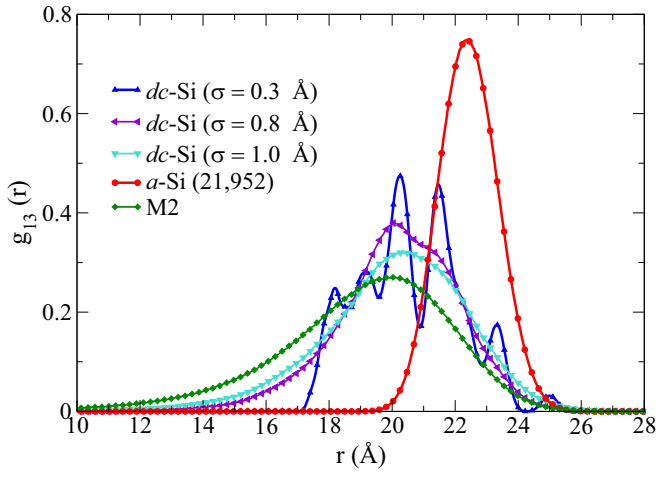

FIG. 8. The shell pair-correlation functions, $g_{13}(r)$, obtained from 21 952-atom WWW models of a-Si (red), dc-Si (blue, purple, and cyan), and partially ordered configurations M2 (green) of Si atoms. The disordered crystalline structures were generated from the diamond c-Si structure, using $\sigma = 0.3$, 0.8, and 1.0 Å.

peaks in $g_{13}(r)$ for dc-Si models. However, as the value of σ increases and goes beyond 0.6 Å, the peaks in $g_{13}(r)$ coalesce to form a unimodal distribution. This is unsurprising due to the presence of strong residual crystalline order in the dc-Si networks for $\sigma \leqslant 0.6$ Å. By contrast, the width of $g_{13}(r)$ for a-Si is found to be considerably smaller than its M2 counterpart, which shows a more radially disordered distribution of atoms within the same shell in M2. This observation is found to be true not only for $g_{13}(r)$ but also for all $g_n(r)$s. The high asymmetry of $g_{13}(r)$ for the M2 and dc-Si models can be readily attributed to the connectivity of the atoms in these models. Since the position of an atom in a given coordination shell is determined by the number of steps or hops from the central atom, there exist a few atoms in the shell that are radially close to the central atom but are not reachable (from the central atom) via a small number of steps or hops, due to the low connectivity of the atoms in the networks for increasing values of σ. This is reflected in the left tail of the distribution (see Fig. 8), which leads to a negative value of the skewness for the radial distribution of atoms in the shell. This can be verified by computing the Fisher-Pearson (FP) coefficient of skewness [50], s, for $g_{13}(r)$, for different σ values. In general, the FP coefficient of skewness is given by the standardized third central moment of a distribution, and a negative value of the coefficient signifies a skewed distribution toward the left, and vice versa. The variation of s with σ for a number of dc-Si models is shown in Fig. 9, along with the corresponding value of the coefficient for the M2 and a-Si model for comparison.

Figure 10 shows the full width at half maximum (FWHM) of the shell PCFs, $g_n(r)$, for different shells, from $n = 1$ to $n = 20$, for a class of partially ordered models (M1–M3), a-Si, and dc-Si models of size 21 952 atoms. Since dc-Si models tend to exhibit the presence of multiple peaks in $g_n(r)$ for $\sigma \leqslant 0.6$ Å, the FWHM for the dc-Si models (with multiple peaks) in Fig. 10 is calculated by fitting each individual peak with a Gaussian distribution and averaging over the resulting FWHM values for all major peaks in the distribution. The

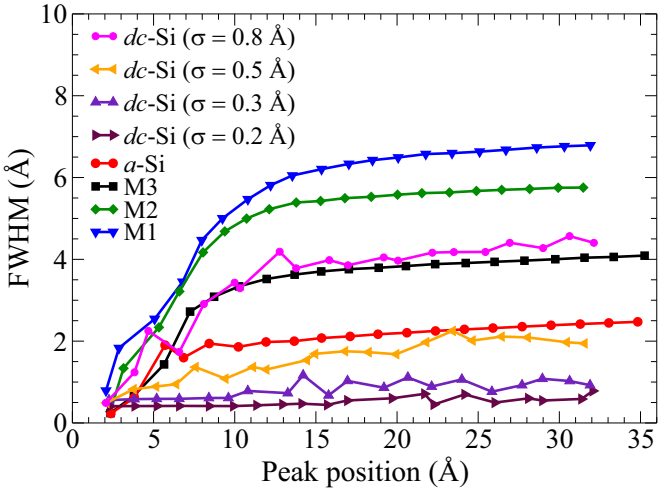

FIG. 10. The full width at half maximum (FWHM) for a set of partially ordered configurations (M1–M3), a-Si, and four dc-Si structures of size 21 952 atoms. The dc-Si structure (with $\sigma = 0.2$ Å) is the most ordered configuration, whereas M1 is the least ordered configuration, by construction.

FWHM values (in Fig. 10) suggest that the M1 models are highly disordered, whereas the dc-Si structures with $\sigma = 0.2$ Å are the least disordered configurations. This observation is indeed true by construction. For $\sigma = 0.2$–0.5 Å, a significant radial ordering exists in the dc-Si structures that leads to a small value of the width in Fig. 10. The rest of the models, from M2 and M3 to a-Si, exhibit an increasingly more ordered state of radially distributed atoms in the shells. It is apparent that, as more radial ordering is incorporated in a model (for example, M2 and M3), the corresponding FWHM value of $g_n(r)$ begins to decrease for a given shell. Conversely, the inclusion of (additional) structural disorder increases the corresponding FWHM value of $g_n(r)$ in a model. This can be seen from Fig. 11, where the addition of positional disorder, via

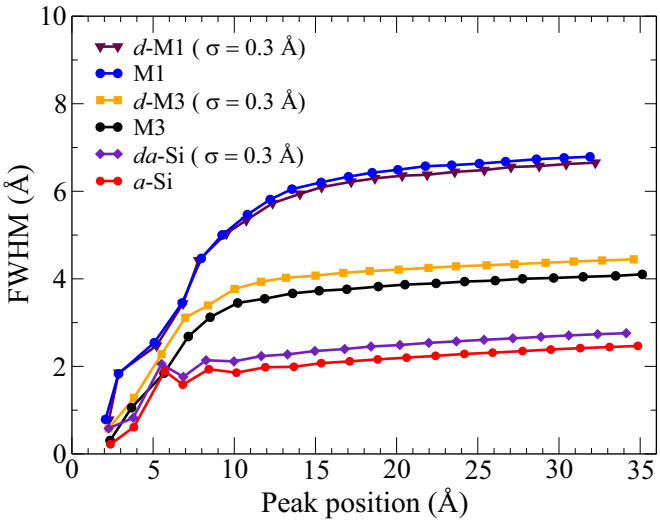

FIG. 11. The effect of the addition of positional disorder on the FWHM of the shell PCFs in M1, M3, and a-Si. The FWHM values of the unperturbed models are also shown for comparison.

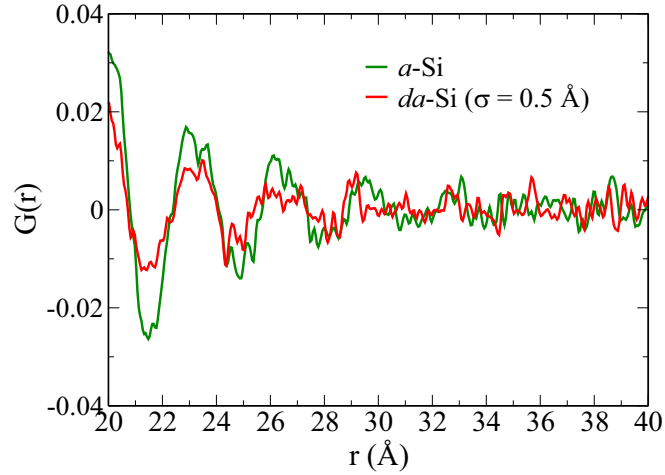

FIG. 12. The effect of the addition of positional disorder, with $\sigma = 0.5$ Å, on the radial oscillations in a 400 000-atom MD model of a-Si between 20 and 40 Å. The results for the corresponding pristine a-Si model (green) are also shown for comparison.

random displacements of atoms in M1, M3, and a-Si, resulted in an increase of the FWHM values of $g_n(r)$. This observation also applies to the total PCF of a-Si. Figure 12 shows that the amplitude of the radial oscillations reduces in the region of 20–40 Å with the addition of positional disorder in a-Si. It may be noted that the FWHM values for the M1 models, which are highly disordered by construction, are practically unaffected in Fig. 11 in the presence of additional disorder with σ values of the order of 0.3 Å. Thus, the width (or the average width for a multimodal case) of $g_n(r)$ can be taken as a measure of the radial order or disorder in partially ordered networks, including a-Si and dc-Si structures.

C. Shannon information as a measure of extended-range ordering

The assertion that the width of the shell pair-correlation function, $g_n(r)$, can provide a measure of the disorder in the radial distribution of atoms in the nth coordination shell of a disordered network is not particularly surprising and it directly follows from the Shannon measure of information (SMI) [51]. By normalizing the shell PCF, $g_n(r)$, one can readily construct a discrete probability measure, p_n^i, to define the SMI as follows:

$$S[p_n^i] = -k \sum_i p_n^i \ln p_n^i. \tag{4}$$

In Eq. (4), the value of $0\ln(0)$ is defined to be 0, k is a constant, and p_n^i is given by

$$p_n^i = \frac{g_n(r_i)}{\sum_i g_n(r_i)}.$$

The SMI can be understood as providing a measure of the degree of uncertainty or the lack of radial ordering in the distribution of atoms in the coordination shells. The multiplicative constant k in Eq. (4) can be taken as unity without any loss of generality. The results for the SMI obtained from M1, M2, M3, and a-Si models are shown in Fig. 13 for the first

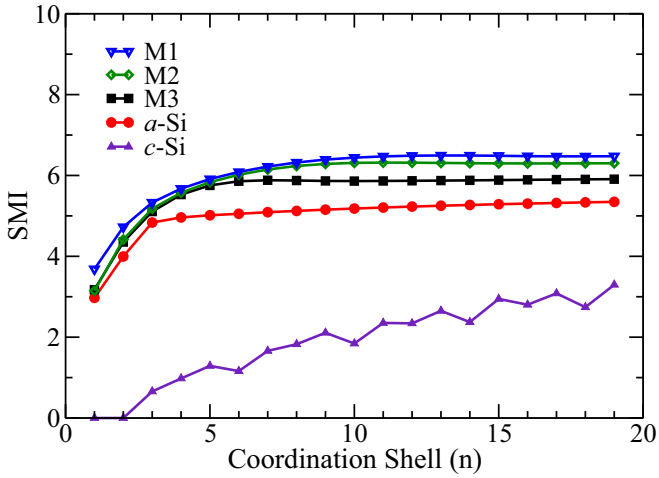

FIG. 13. The Shannon measure of information (SMI), associated with a discrete probability measure p_n, obtained from the shell pair-correlation functions, $g_n(r)$, for M1–M3, a-Si, and diamond c-Si. For disordered and amorphous Si networks, the results were averaged over three independent configurations for each shell.

20 coordination shells. The corresponding results for diamond c-Si are also shown in the plot for comparison. As one may expect, the SMI values for different shells behave in a similar manner as that of the FWHM (of the shell PCFs) with respect to the peak position in Fig. 10. Once again, the largest values of the SMI correspond to the highly disordered M1 models, whereas a-Si exhibits the smallest values of the SMI for each shell among M1, M2, M3, and a-Si. It is noteworthy that, unlike the case of disordered and amorphous Si networks, the SMI values associated with the coordination shells in the diamond c-Si structure, which is perfectly ordered, increase considerably with the increasing shell number in a global sense. This observation can be attributed to the presence of multiple peaks in the higher-order coordination shells. Since the (shell) PCFs for a crystalline structure consist of a series of δ functions, the presence of an increasing number of peaks in the distant shells leads to more uncertainty in the radial distribution of the atoms in these shells. This is reflected in the larger value of the SMI for the distant shells. Thus, the SMI can be loosely interpreted as a global measure of ordering or disordering in the distribution, which is most appropriate for describing the degree of order or disorder associated with unimodal distributions. However, for multimodal distributions, such as the dc-Si structures with $\sigma \leqslant 0.5$ Å, one requires a suitable local measure of information, for example, the Fisher information [52], in order to quantify the degree of disorder or uncertainty associated with the radial distribution of the atoms in the coordination shells. These issues will be addressed elsewhere from an information-theoretic point of view in a future communication.

The origin of the extended-range oscillations in a-Si can now be interpreted in light of the results from Figs. 7–13. Since the full PCF can be expressed in terms of its partial components, any structural aspects of $g(r)$, such as the extended-range oscillations, can also be represented by a suitable set of $g_n(r)$, associated with the length scale of the oscillations. Figures 10 and 13 essentially suggest that, as the degree of radial ordering in the full PCF increases from M1 to M3, the corresponding width and the Shannon information associated with $g_n(r)$ steadily decrease. Thus, the inclusion of radial information of up to a distance of 4 Å in M2 and about 6 Å in M3 suffices to result in a reduction of the width of $g_n(r)$ associated with the distant coordination shells. Since a-Si is characterized by the presence of strong radial ordering at least up to a length of 20 Å in the full PCF, it is unsurprising that a small value of the width of $g_n(r)$ of a-Si is reflective of the radial ordering in the distant shells on the length scale of 20–40 Å. By contrast, the dc-Si models with $\sigma = 0.2$–0.5 Å show significant radial ordering as far as the widths of various $g_n(r)$s are concerned. Thus, the ERO in a-Si can be understood as the resultant density fluctuations, originating from highly ordered radial distributions of atoms in the first few coordination or radial shells, which propagate and decay radially as the (density) fluctuations travel through the distant shells. A comparison of the results from the M2, M3, and a-Si models in Fig. 10 appears to suggest that the characteristic local radial ordering of up to 6 Å forces the atoms in distant shells to organize in such a way that small radial oscillations are built up on the length scale of up to 40 Å, when the model is sufficiently large. The presence of these small but distinct radial oscillations in the full PCF is indicative of the existence of weak extended-range radial ordering in a-Si up to a length of 40 Å, as far as the size of the a-Si models studied in this work are concerned.

D. Decay of radial correlations, autocorrelation coefficient, and comparison with experimental diffraction data

The presence of radial atomic correlations beyond 20 Å can be further evidenced by computing the autocorrelation coefficient(s) of $G(r)$. Assuming that M observations, y_1, y_2, ..., y_M, form a time series, where $y_i = G(r_i)$, the autocovariance coefficient [53], c_k, between the observations that are k steps apart is given by

$$c_k = \frac{1}{M}\sum_{i=1}^{M-k}(y_i - \bar{y})(y_{i+k} - \bar{y}),\ k = 1, \ldots, n, n < M. \quad (5)$$

The autocorrelation coefficient, γ_k, is then expressed as $\gamma_k = c_k/c_0$, where c_0 is the variance and $\bar{y}$ is the mean value of the set $\{y_i\}$. Figure 14 shows a plot of γ_k versus r_k. Here, the set $\{y_i\}$ is constructed by choosing a segment of $G(r)$ from $r_1 = 15$ Å to $r_n = 45$ Å and expressing k in terms of $r_k = r_1 + k\Delta r$, where Δr is the distance between two consecutive observations of $G(r)$. It is apparent from the plot that, given the set of $G(r)$ values from 15 to 45 Å, $\Delta r = 0.05$ Å, $n = 600$, and $M = 900$, the radial correlations decay in an oscillatory manner and become almost negligible after 35 Å. The root-mean-square (RMS) fluctuations of γ_k, obtained from the configurational averaging of the results from three independent MD models of size 400 000 atoms, are also shown in Fig. 14. Since the RMS values of the fluctuations are almost of the order of γ_k for $r \geqslant 40$ Å, the radial correlations in this region may not be significant, even though the presence of small residual correlations can be seen in this region.

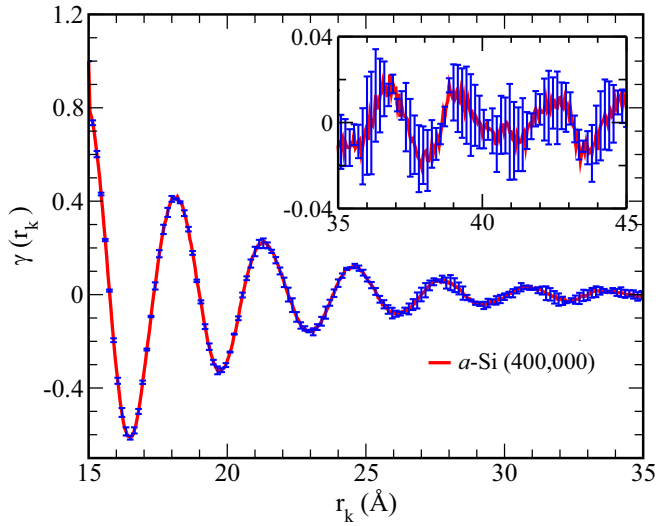

FIG. 14. The autocorrelation coefficient, $\gamma(r_k)$, of a set of $G(r)$ values from $r = 15$ Å to $r = 45$ Å, constructed from 400 000-atom MD models of a-Si, showing the presence of radial correlations up to 45 Å. The root-mean-square fluctuations are shown as error bars (blue vertical lines). For visual clarity, the results for the radial region from 35 to 45 Å are shown in the inset.

We now provide a direct comparison of our results with those from diffraction measurements by computing the decay length and the (spatial) period of the ERO at radial distances beyond 10 Å. High-energy x-ray diffraction measurements on a-Si samples, by Roorda *et al.* [33], suggest that the period of oscillations ranges from 2.77 to 3.03 Å and that the decay length in annealed samples of a-Si is about 4.23 Å. Figure 15 shows the decay of the amplitudes of radial oscillations in $G(r)$ for 400 000-atom MD models of a-Si, which can be roughly considered as the simulated counterpart of annealed

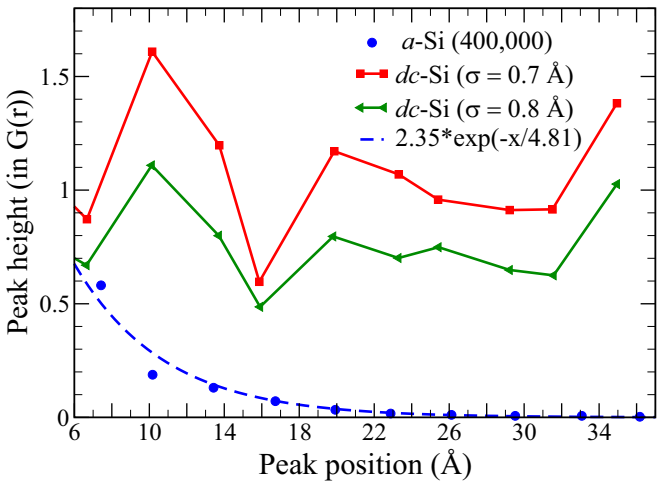

FIG. 15. The decay of the radial peak heights in $G(r)$ for a-Si (blue) and dc-Si (red and green) with peak distances. The exponential fit of the peak positions (dashed blue line) corresponds to the data for a-Si models of size 400 000 atoms. The decay length for a-Si corresponds to a value of 4.81 Å. The corresponding peak positions for dc-Si structures are shown for comparison.

samples of a-Si in experiments. Here, the amplitudes and positions of the peaks are obtained from Fig. 2. The corresponding decay for dc-Si networks for $\sigma = 0.7$ and 0.8 Å are also included in the plot for comparison. For visual clarity, the first three peaks of a-Si are omitted from the plot, by choosing an appropriate range for the y axis. The values of the period and the decay length obtained from our calculations compare very well with the results from experiments. The average period of oscillations from 400 000-atom MD models, in Fig. 15 (and Fig. 2), is found to be 3.2 ± 0.065 Å, which is very close to the experimental value of 3.03 Å, and the corresponding decay length turns out to be about 4.81 ± 0.012 Å. The latter is somewhat higher than the experimental value of 4.23 Å, obtained from the Fourier transform of experimental diffraction data by Roorda *et al.* [33]. It is evident from Fig. 15 that the dc-Si models exhibit a rather slow decay, even for considerably large values of σ from 0.7 to 0.8 Å.

E. Relation between ERO and the first sharp diffraction peak in a-Si

In this section, we address the question whether the presence of extended-range oscillations has any bearing on the position and intensity of the first sharp diffraction peak (FSDP) in a-Si. Since the origin of the FSDP is strongly related to the presence of medium-range order (MRO) in glasses, which can extend up to a radial distance of approximately 20 Å, it is instructive to examine whether the ERO in a-Si can produce any observable effect on the intensity of the FSDP near 2.0 Å^{-1}.

The effect of distant radial correlations on the position and intensity of the FSDP in a-Si can be calculated from using Eq. (1). However, a direct application of Eq. (1) to very large models can be problematic for two reasons. First, the presence of noise in $G(r)$ at large R can introduce errors, depending on the signal-to-noise ratio in $G(r)$. This makes it difficult to identify the optimal value of R_c for large models, by varying the upper limit of the integral in Eq. (1). Second, for large values of R, the integrand can be highly oscillatory and conventional integration techniques may not suffice to accurately compute $S(Q_0)$ in the presence of a noisy $G(r)$. To ameliorate these issues, we address the problem by expressing $G(r)$ in terms of suitable distance-dependent radial basis functions, and calculate the resulting integral analytically to obtain a closed expression for $S(Q)$. Noting that the oscillations are particularly pronounced in $G(r)$, it is useful to write $G(r)$ as a linear combination of Gaussian functions,

$$G(r) = \sum_{i=1}^{m} a_i e^{-b_i(r-c_i)^2}, \tag{6}$$

in an effort to obtain an analytical expression for $S(Q)$ in terms of the Gaussian parameters. The parameters a_i, b_i, and c_i determine the approximate peak and/or trough height, width, and the (radial) position of the ith peak and/or trough, respectively, and can be obtained either via a nonlinear fit of Eq. (6) to experimental or simulated reduced PCF data, $G(r)$, or by minimizing a suitable cost function with respect to the set of parameters (a_i, b_i, c_i). Here, we have taken the second approach and ensured that $b_i > 0$ for all i. The structure factor can be expressed in terms of the fitted Gaussian

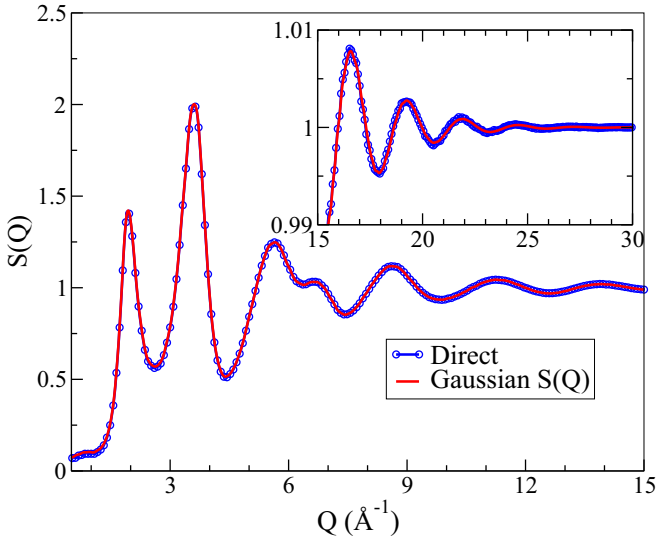

FIG. 16. The static structure factor, $S(Q)$, of a 21 952-atom WWW model of a-Si obtained from the Gaussian approximation (red line) and from direct numerical calculations (blue circles) using Eqs. (8) and (7), respectively.

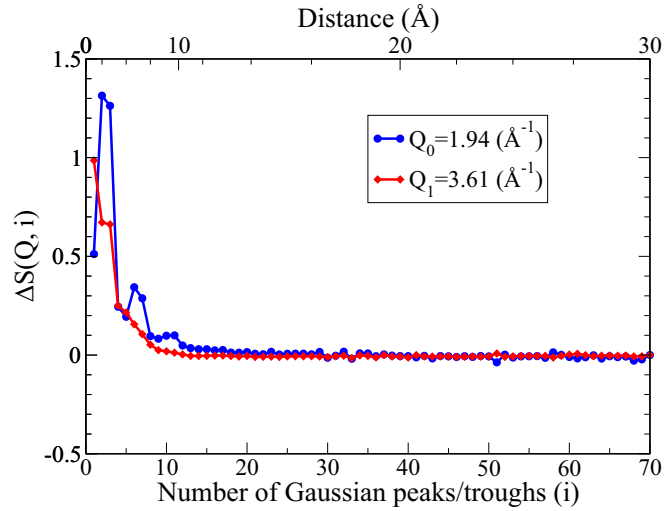

FIG. 17. The convergence of the intensity of the FSDP (at Q_0) and the principal peak (at Q_1), obtained from Eq. (8), with respect to the number (i) of Gaussian peaks and/or troughs for a 21 952-atom WWW model. The radial length associated with the Gaussian peaks and/or troughs is indicated in angstroms on the secondary x axis (top).

parameters:

$$S(Q) = 1 + \int_0^{R_c} rG(r)\,\frac{\sin(Qr)}{Qr}\,dr \tag{7}$$

$$= 1 + \frac{1}{Q}\sum_{i=1}^{m} a_i\sqrt{\frac{\pi}{b_i}}\,\sin(Qc_i)\,\exp\left[-\frac{Q^2}{4b_i}\right]. \tag{8}$$

In writing Eq. (8), we have denoted, for notational convenience, the set (a_i, b_i, c_i) as the fitted values of the parameters and assumed that the center of each Gaussian function, c_i, satisfies the condition $0 \ll c_i \ll R_c$ so that $S(Q)$ can be written as a sum of Gaussian integrals (and not error functions) with the integration limit extending from zero to ∞. This condition is readily satisfied by choosing an appropriate value of m, such that $R_c \gg c_m$, and noting that the first peak of the PCF in a-Si rapidly decays to zero for $r \leqslant 2.0$ Å. In practical calculations, a value of R_c of the order of 20 Å is found to be sufficient for accurate determination of $S(Q)$ using Eq. (7) [see Dahal *et al.* [54] and Fig. 16 here]. The structure factor obtained from Eq. (8) for a 21 952-atom WWW model of a-Si is plotted in Fig. 16, along with the results from direct numerical calculations from Eq. (7) for comparison. For clarity, the wavevector region from 15 to 30 Å^{-1} is shown separately as an inset in Fig. 16.

The variation of the intensity of the FSDP and the principal peak (i.e., the peak at 3.6 Å^{-1}) can be studied, by using Eq. (8), with respect to the number of Gaussian basis functions m for a given R_c. Writing $\Delta S(Q, i) = S(Q, m) - S(Q, i)$, where $m = 70$ for $R_c = 30$ Å, Fig. 17 shows the convergence of ΔS at $Q_0 = 1.94$ Å^{-1} and $Q_1 = 3.6$ Å^{-1} for an increasing number (i) of peaks and/or troughs. Here, Q_0 and Q_1 correspond to the position of the FSDP and the principal peak, respectively. It is apparent that both $S(Q_0, i)$ and $S(Q_1, i)$ converge to the respective limiting value, $S(Q, m)$, very rapidly as i approaches 30, which corresponds to a radial length of about 18 Å, as indicated in Fig. 17. The length is indicated at the top of the plot as a secondary x axis, which reflects the nonuniform distribution of Gaussian peaks and/or troughs in the radial region of 0–30 Å. Figure 17 suggests that radial correlations from the region beyond 20 Å do not really play any significant role. This observation can be stated more precisely. The magnitude of the contribution to $S(Q)$ obtained by including an additional peak or trough beyond m in Eq. (8) can be written as

$$|\delta S(Q, m)| = |S(Q, m+1) - S(Q, m)|$$

$$= \left|\frac{1}{Q}\sqrt{\frac{\pi a_{m+1}^2}{b_{m+1}}}\,\sin(Qc_{m+1})\,\exp\left[-\frac{Q^2}{4b_{m+1}}\right]\right|$$

$$\leqslant \frac{1}{Q}\sqrt{\frac{\pi a_{m+1}^2}{b_{m+1}}}\,\exp\left[-\frac{Q^2}{4b_{m+1}}\right]. \tag{9}$$

Substituting $Q = Q_0 = 2$ Å^{-1} in Eq. (9) for the FSDP in a-Si, one obtains

$$|\delta S(Q_0, m)| < \frac{a_{m+1}}{\sqrt{b_{m+1}}}\,\exp\left[-\frac{1}{b_{m+1}}\right]. \tag{10}$$

The asymptotic behavior of $|\delta S(Q_0, m)|$ with respect to m follows from Eq. (10). Since $G(r) \to 0$ as $r \to R_c$ for very large models, the parameter a_m, which determines the height of the Gaussian peak, decreases with an increasing value of m, and $|\delta S(Q_0, m)|$ becomes increasingly smaller as m becomes a large number. In practice, however, $|\delta S(Q_0, m)|$ fluctuates between zero and a small value ϵ due to the presence of numerical noise at large radial distances, which can be reduced by averaging $S(Q)$ [in Eq. (8)] over many independent sets of fitted Gaussian parameters. Further, a value of R_c of about 30 Å is found to be sufficient for the calculation of $S(Q)$ from Eqs. (7) and (8). The results from our calculations suggest that the average value [55] of ϵ is typically of the order of 0.025 for

radial distances between 20 and 30 Å. This roughly translates into an error of 1.7%, assuming $S(Q_0) = 1.5$ for as-deposited samples from experiments [8]. Thus, aside from small fluctuations of $S(Q_0)$ owing to numerical noise, the extended-range oscillations in the radial region of 20–30 Å do not seem to play any observable role in determining the intensity of the FSDP in *a*-Si. A similar conclusion was reached in a recent study [54], where an alternative argument based on the analysis of the behavior of $rG(r)$ and the sampling of $\sin(Qr)/Qr$ within the radial region from zero to R_c in Eq. (7) was provided by the authors of the study to support this conclusion.

IV. CONCLUSIONS

The present study addresses the origin of the extended-range oscillations in *a*-Si from a real-space point of view. By analyzing a class of large partially ordered networks of Si atoms with radial ordering up to a distance of 6 Å in the PCF, it has been shown that the inclusion of short-range ordering in the first two coordination shells of the disordered networks can lead to an increased ordering of the atomic radial distribution in distant coordination shells. A comparison of these results with those obtained from large *a*-Si and disordered crystalline configurations reveals that the shell pair-correlation functions for the coordination shells of *a*-Si at radial distances of 20–30 Å are considerably ordered and that this radial ordering manifests in the form of weak oscillations in the total PCF of *a*-Si, which can be expressed as a sum of the partial radial distributions from each coordination shell. By using the full width at half maximum of the peak(s) of the partial PCFs and the Shannon information as a measure of the degree of order or disorder, one arrives at the conclusion that local atomic correlations can considerably affect the distribution of atoms in *a*-Si up to a distance of 40 Å.

An analysis of the amplitude of radial oscillations in the reduced PCF of 400 000-atom MD models of *a*-Si shows that the envelope function of the reduced PCF decays almost exponentially and the resulting decay length (of 4.81 Å) is found to be close to the experimental value (of 4.23 Å), estimated from the Fourier transform of the diffraction data obtained for annealed samples of *a*-Si. Likewise, the period of the extended-range oscillations (for MD models) is found to be about 3.2 Å, which compares well with the corresponding experimental value of 3.03 Å for annealed samples. The study also shows that the structure factor of *a*-Si can be expressed as a linear combination of a series of Gaussian functions, whose amplitude is modulated by a sinc function. A convergence study of the intensity of the FSDP, using the structure factor obtained from the Gaussian approximation, with respect to the number of peaks in real space shows that the structure of the FSDP is primarily determined by the radial correlations originating from a distance of up to 20 Å in *a*-Si networks, which leads to the conclusion that the ERO has no discernible effects on the FSDP in *a*-Si.

ACKNOWLEDGMENTS

The work was partially supported by the U.S. National Science Foundation (NSF) under Grant No. DMR 1833035. One of us (P.B.) thanks Dr. Raymond Atta-Fynn for discussions.

There are no conflicts of interest to declare.

[1] W. H. Zachariasen, J. Am. Chem. Soc. **54**, 3841 (1932).
[2] S. R. Elliott, Nature (London) **354**, 445 (1991).
[3] P. Biswas, D. Paudel, R. Atta-Fynn, and S. R. Elliott, Nanoscale **12**, 1464 (2020).
[4] P. Biswas and S. R. Elliott, J. Phys.: Condens. Matter **27**, 435201 (2015).
[5] D. Dahal, R. Atta-Fynn, S. R. Elliott, and P. Biswas, J. Phys.: Conf. Ser. **1252**, 012003 (2019).
[6] J. M. Gibson and M. M. J. Treacy, Phys. Rev. Lett. **78**, 1074 (1997).
[7] A. Uhlherr and S. R. Elliott, J. Phys.: Condens. Matter **6**, L99 (1994).
[8] R. Xie, G. G. Long, S. J. Weigand, S. C. Moss, T. Carvalho, S. Roorda, M. Hejna, S. Torquato, and P. J. Steinhardt, Proc. Natl. Acad. Sci. U.S.A. **110**, 13250 (2013).
[9] M. Aniya and F. Shimojo, J. Non-Cryst. Solids **341**, 110 (2004).
[10] B. Shyam, K. H. Stone, R. Bassiri, M. M. Fejer, M. F. Toney, and A. Mehta, Sci. Rep. **6**, 32170 (2016).
[11] Q. Mei, C. J. Benmore, S. Sen, R. Sharma, and J. L. Yarger, Phys. Rev. B **78**, 144204 (2008).
[12] P. S. Salmon, A. C. Barnes, R. A. Martin, and G. J. Cuello, Phys. Rev. Lett. **96**, 235502 (2006).
[13] S. Sampath, C. J. Benmore, K. M. Lantzky, J. Neuefeind, K. Leinenweber, D. L. Price, and J. L. Yarger, Phys. Rev. Lett. **90**, 115502 (2003).
[14] P. Vashishta, R. K. Kalia, G. A. Antonio, and I. Ebbsjö, Phys. Rev. Lett. **62**, 1651 (1989).
[15] J. Phillips, J. Non-Cryst. Solids **43**, 37 (1981).
[16] G. Lucovsky, J. Non-Cryst. Solids **97–98**, 155 (1987).
[17] H. Iyetomi, P. Vashishta, and R. K. Kalia, Phys. Rev. B **43**, 1726 (1991).
[18] P. Armand, A. Ibanez, E. Philippot, Q. Ma, and D. Raoux, J. Non-Cryst. Solids **150**, 371 (1992).
[19] H. W. Sheng, W. K. Luo, F. M. Alamgir, J. M. Bai, and E. Ma, Nature (London) **439**, 419 (2006).
[20] Y. Yang, J. Zhou, F. Zhu, Y. Yuan, D. J. Chang, D. S. Kim, M. Pham, A. Rana, X. Tian, Y. Yao, S. J. Osher, A. K. Schmid, L. Hu, P. Ercius, and J. Miao, Nature (London) **592**, 60 (2021).
[21] D. Ma, A. D. Stoica, and X. L. Wang, Nat. Mater. **8**, 30 (2009).
[22] L. Cormier, P. H. Gaskell, G. Calas, and A. K. Soper, Phys. Rev. B **58**, 11322 (1998).
[23] P. S. Salmon, J. Phys.: Condens. Matter **19**, 455208 (2007).
[24] S. Hazra, I. Sakata, M. Yamanaka, and E. Suzuki, Phys. Rev. B **69**, 235204 (2004).
[25] A. Hirata, P. Guan, T. Fujita, Y. Hirotsu, A. Inoue, A. R. Yavari, T. Sakurai, and M. Chen, Nat. Mater. **10**, 28 (2011).
[26] B. K. Sharma and M. Wilson, Phys. Rev. B **73**, 060201(R) (2006).
[27] K. Tanaka, Jpn. J. Appl. Phys. **37**, 1747 (1998).

[28] K. Nishio, T. Miyazaki, and H. Nakamura, Phys. Rev. Lett. **111**, 155502 (2013).

[29] J. Du and L. R. Corrales, J. Non-Cryst. Solids **352**, 3255 (2006).

[30] V. L. Deringer, N. Bernstein, G. Csányi, C. B. Mahmoud, M. Ceriott, M. Wilson, D. A. Drabold, and S. R. Elliott, Nature (London) **589**, 59 (2021).

[31] J. Fortner and J. S. Lannin, Phys. Rev. B **39**, 5527 (1989).

[32] J. M. Holender and G. J. Morgan, J. Phys.: Condens. Matter **3**, 7241 (1991).

[33] S. Roorda, C. Martin, M. Droui, M. Chicoine, A. Kazimirov, and S. Kycia, Phys. Rev. Lett. **108**, 255501 (2012).

[34] F. Wooten, K. Winer, and D. Weaire, Phys. Rev. Lett. **54**, 1392 (1985).

[35] G. T. Barkema and N. Mousseau, Phys. Rev. B **62**, 4985 (2000).

[36] J. S. Custer, M. O. Thompson, D. C. Jacobson, J. M. Poate, S. Roorda, W. C. Sinke, and F. Spaepen, Appl. Phys. Lett. **64**, 437 (1994).

[37] K. Laaziri, S. Kycia, S. Roorda, M. Chicoine, J. L. Robertson, J. Wang, and S. C. Moss, Phys. Rev. B **60**, 13520 (1999).

[38] R. L. C. Vink, G. T. Barkema, and W. F. van der Weg, Phys. Rev. B **63**, 115210 (2001).

[39] F. H. Stillinger and T. A. Weber, Phys. Rev. B **31**, 5262 (1985).

[40] S. Nosé, J. Chem. Phys. **81**, 511 (1984).

[41] W. G. Hoover, Phys. Rev. A **31**, 1695 (1985).

[42] R. Atta-Fynn and P. Biswas, J. Chem. Phys. **148**, 204503 (2018).

[43] P. N. Keating, Phys. Rev. **145**, 637 (1966).

[44] W. Weber, Phys. Rev. B **15**, 4789 (1977).

[45] See Supplemental Material at http://link.aps.org/supplemental/10.1103/PhysRevB.105.115203 for the atomic coordinates of three WWW models used in this study.

[46] R. Haydock, V. Heine, and M. J. Kelly, J. Phys. C: Solid State Phys. **5**, 2845 (1972).

[47] R. Haydock, in *Solid State Physics*, Vol. 35, edited by H. Ehrenreich, F. Seitz, and D. Turnbull (Academic Press, New York, 1980), pp. 216–287.

[48] In the recursion method, the diagonal element of $\hat{G}(z)$ is computed by transforming the tight-binding H matrix into a tridiagonal form using the Lanczos algorithm and expressing the element as a continued fraction. The coefficients of the continued fraction are determined by the diagonal and off-diagonal elements of the tridiagonal matrix, and a suitable terminator scheme, which preserves the analytic properties of $\hat{G}(z)$, is used to evaluate the continued fraction.

[49] P. Biswas, Phys. Rev. B **65**, 125208 (2002).

[50] The Fisher-Pearson coefficient of skewness of a distribution, $p(x)$, is expressed as the standardized third central moment, $E[((x-\mu_1)/v)^3]$,where μ_n is the conventional nth moment and $v^2 = \mu_2 - \mu_1^2$ of $p(x)$. For samples of finite size, n, one often multiplies by a scale factor of $\sqrt{n(n-1)}/(n-2)$ to obtain the adjusted Fisher-Pearson coefficient. The value of the adjusted coefficient is reported in this study.

[51] C. E. Shannon, Bell Syst. Tech. J. **27**, 379 (1948).

[52] R. A. Fisher, *Statistical Methods, Experimental Design, and Scientific Inference* (Oxford University Press, Oxford, 1959).

[53] The covariance is expressed as the average cross product between two variables. One often uses M-k instead of M in the denominator of Eq. (5). However, this does not affect the results for $n \ll M$.

[54] D. Dahal, H. Warren, and P. Biswas, Phys. Status Solidi B **258**, 2000447 (2021).

[55] Owing to the stochastic nature of the minimization problem in fitting Eq. (6) with simulated $G(r)$ of a-Si, we have used here 20 independent sets of Gaussian parameters, (a_i, b_i, c_i), to obtain a robust estimate of the average value of ϵ.